Research Paper

Liquefaction during the Kumamoto Earthquakes on April 14 and 16, 2016

K. Wakamatsu[1], S. Senna[2] and K. Ozawa[3]

ARTICLE INFORMATION

ABSTRACT

At 21:26 JST on April 14, 2016, an earthquake with a Japan Metrological Agency Magnitude (M_{JMA}) of 6.5 struck Kumamoto Prefecture, Kyushu, in southwestern Japan. This earthquake was followed by a larger earthquake with an M_{JMA} of 7.3 at 1:25 JST on April 16, 2016. These were the most severe earthquakes to occur in Japan since the Tohoku earthquake in 2011. The hypocenters of the strike-slip M_{JMA} 6.5 foreshock and M_{JMA} 7.3 main shock and, along with the aftershocks, were widely distributed along the active Futagawa-Hinagu strike-slip fault. This paper first presents the distribution of the liquefied sites during these earthquakes and their effects on the surrounding buildings and infrastructure. Next, the distance from the epicenter to the farthest liquefied site is compared with past Japanese earthquakes, followed by a discussion on the intensities of the ground motion that caused the liquefaction. Finally, the land conditions and soil profiles where severe and widespread liquefaction occurred are investigated.

1. Introduction

At 21:26 JST on April 14, 2016, a Japan Metrological Agency Magnitude (M_{JMA}) 6.5 earthquake struck Kumamoto Prefecture, Kyushu, in southwestern Japan. This earthquake was followed by a larger earthquake of M_{JMA} 7.3 at 1:25 JST on April 16, 2016. These were the most severe earthquakes to affect Japan since the Tohoku earthquake in 2011. The hypocenters of the strike-slip M_{JMA} 6.5 foreshock and M_{JMA}7.3 main shock and its aftershocks were widely distributed along the Hinagu-Futagawa active fault (National Research Institute for Earth Science and Disaster Resilience, 2016). Both earthquakes registered a reading of 7 on the Japan Metrological Agency seismic intensity scale (I_{JMA}), which is the highest I_{JMA} reading recorded in the town of Mashiki,

approximately 6.5 and 5.5 km from the epicenters of the main shock and foreshock, respectively.

The earthquakes elicited a strong response, and significantly damaged homes and infrastructure. As of March 14, 2017, 8,673 houses in the Kumamoto Prefecture have been destroyed, and numerous landslides have occurred in the Mt. Aso area, which is approximately 30 km northeast of the hypocenter of the main shock (Cabinet Office, 2016). Our liquefaction field reconnaissance surveys and interpretation of the high-resolution aerial photographs taken immediately after the earthquakes revealed that the earthquakes induced liquefaction at a considerable number of locations in an 80-km long zone, extending along the faults in Kumamoto Prefecture.

This paper presents the distribution of the liquefied sites and their effects on the surrounding buildings and

[1]Professor, Department of Civil Engineering,Kanto Gakuin University, Yokohama, Kanagawa, 236-8501, JAPAN, wakamatu@kanto-gakuin.ac.jp
[2]Principal Researcher, Department of Integrated Research on Disaster Prevention,National Research Institute for Earth Science and Disaster Resilience, Tsukuba, Ibaraki, 305-0006 JAPAN, senna@bosai.go.jp
[3]Researcher,Department of Integrated Research on Disaster Prevention,National Research Institute for Earth Science and Disaster Resilience,Tsukuba, Ibaraki, 305-0006 JAPAN, kyoko@bosai.go.jp
Note: Discussion on this paper is open until June 2018

192

K. Wakamatsu et al. / Lowland Technology International 2017; 19 (3): 191-202
Special Issue on: Kumamoto Earthquake & Disaster
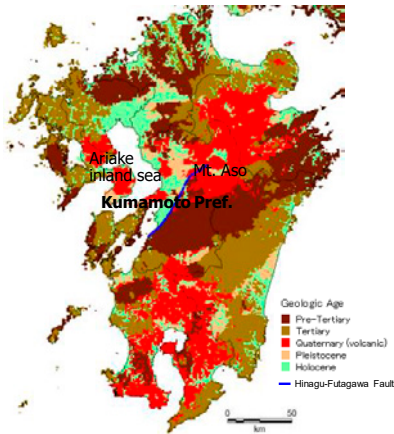
Fig. 1. Surface geology of Kyushu (Wakamatsu et al., 2005) and the Hinagu-Futagawa Fault (The Headquarters for the Earthquake Research Promotion, 2016)

Fig. 2. Liquefied sites during the 2016 Kumamoto Earthquake

infrastructure during the earthquake. Additionally, the distance from the epicenter to the farthest liquefied site is compared with previous Japanese earthquakes, and the intensities of ground motion that caused the liquefaction are discussed. Finally, the land conditions and soil profiles where severe and widespread liquefaction occurred are investigated.

2. Geology and tectonics of affected area

Figure 1 shows a geological map of Kyushu, the southernmost of the four major Japanese islands. Kumamoto Prefecture, which was the earthquake-stricken area, is located at the center of Kyushu. The land features of Kumamoto Prefecture are characterized by Mt. Aso (1,592 m in height), an extensively active volcano located in the east, pre-tertiary mountain ranges running along the SW-NE direction in the south, and the Holocene, extending to the western areas facing the Ariake inland sea.

A series of earthquakes in Kumamoto Prefecture were induced by a slippage of a 6-km-long northwestern segment of the 81-km-long Hinagu Fault, and a 28-km long northwestern segment of the 64-km-long Futagawa Fault. Based on the distribution of aftershocks and the focal mechanism of the main shock, the source fault was estimated to be a right-lateral strike-slip fault extending in the NNE-SSW direction (Headquarters for Earthquake Research Promotion, 2016).

3. Liquefaction observed during the 2016 Kumamoto earthquake

3.1 Distribution of liquefied sites

Through our investigations, occurrences of liquefaction were identified based on the sand and water boiling

observed during field reconnaissance surveys, and on an interpretation of aerial photos taken immediately after the earthquake. During the investigations, liquefaction of the backfill soil (e.g., sewage pipelines, manholes, and levee body material) was excluded from the study because it was not ground-condition related.

Figure 2 shows the distribution of the liquefied sites during the Kumamoto earthquake. The red dots in **Fig. 2** represent the sites where sand boil deposits were observed in our field reconnaissance surveys during April 28 to May 1, May 11 to 12, and May 21 to 22. The green dots show liquefied sites induced by the foreshock on April 14, and the blue dots show the liquefied sites additionally generated by the main shock on April 16. The sand and water boiling occurring at the sites, shown in the green and blue dots, were identified through the interpretation of satellite images from Google Earth taken immediately after the foreshock, and high-resolution aerial images taken immediately after the main shock on April 16 (Geospatial Information Authority of Japan, 2016), respectively. Namely, the green points were confirmed before the main shock on April 16 occurred. Comparing the two sets of images taken on April 15 (shots of the April 14 foreshock were taken on April 15) and April 16, the size of the sand boil deposits from the April 15 shots were enlarged in the April 16 shots, as shown in **Figs. 3(a)** and **3(b)**, thus implying that the liquefied sites during the foreshock were repeatedly liquefied during the main shock on April 16.

Liquefaction occurred in an 80-km long zone extending along the Hinagu-Futagawa fault in 18 cities, towns, and villages in Kumamoto Prefecture. The liquefaction in the eastern areas of the prefecture, including the Aso region, occurred during the main shock. Counting the numbers of grid cells containing any liquefaction site, which were determined by superimposing 250-m grid cells, 404 and 1,890 grid cells were designated as "liquefied grid-cells" for the foreshock on April 14 and the main shock on April

(a) After the foreshock on April 14 (Source Google Earth of April 15)

(b) After the main shock of April 16 (Geospatial Information Authority of Japan, 2016). Building A and B with spread foundation were settled due to liquefaction.

Fig. 3. Sand boiling at a shopping mole in Kashima-machi (32.739032N, 130.741351E)
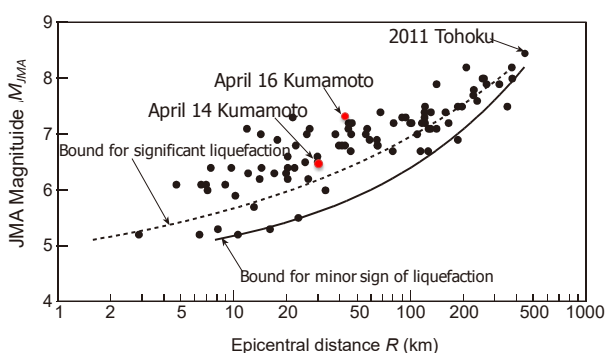
Fig. 4. Epicentral distance to farthest liquefied sites, R, in km for Japan Metrological Agency Magnitude, M_{JMA}

16, respectively. Approximately one-third of the liquefied grid-cells for the main shock were found within the Aso region located inside the outer crater of Mt. Aso.

3.2 Liquefied site farthest from the epicenter

Several investigators have analyzed the distribution of liquefaction during previous earthquakes, and have compared the distance from the epicenter to the farthest liquefied site, R, with respect to the earthquake magnitude, M (Kuribayashi and Tasuoka, 1975; Ambraseys, 1988; Wakamatsu, 1991 and 2011). In the case of the Kumamoto Earthquake, Ohama, located in Tamana City, northwest of Kumamoto City, was the farthest site of liquefaction from the epicenter of the M_{JMA} 6.5 foreshock, the epicentral distance of which was 29.6 km. The farthest site from the epicenter of the main M_{JMA} 7.3 shock was Ichinomiya, in Aso City, the epicentral distance of which was 42.6 km.

Figure 4 shows the empirical relationships between the earthquake magnitude, M_{JMA}, and epicentral distance, R, to the farthest liquefied sites derived from 87 Japanese earthquakes used to estimate the maximum extent of liquefaction in a susceptible area during an earthquake (Wakamatsu, 2011). The values of M_{JMA} versus R for the

sites of liquefaction caused by the foreshock and main shock are plotted in **Fig. 4**. Both distances are within the limiting boundary for significant liquefaction given by Wakamatsu (2011), which indicates that the maximum extent of liquefaction during the foreshock and main shock of the Kumamoto earthquake were not large in relation to the earthquake magnitude, when compared with past Japanese earthquakes.

3.3 Liquefaction-induced damage

Liquefaction caused considerable damage to residential structures, agricultural land and facilities, river levees, roads, and lifelines. Kumamoto City reported that

Fig. 5. Fissure ejecting black sand along former river (Kojima Park, Nishi-ku, Kumamoto City, 32.776476N, 130.635140E)

Fig. 6. Tilted wall due to liquefaction (Chikami, Minami-ku, Kumamoto City, 32.770945N, 130.692849E)

Fig. 7. Sandbags refilled with 25 kg sand boil deposits removed from a 4 meter-deep well. The number of sandbags reached 320 in total (8 ton in weight) (Chikami, Minami-ku, Kumamoto City, 32.769953N, 130.691958E)

Fig. 8. A five-story building constructed three years ago lifted because of a 1-m ground subsidence (Chikami, Minami-ku, Kumamoto City, 32.769215N, 130.691603E)

Fig. 9. An electric pole settled by more than 1 meter (Chikami, Minami-ku, Kumamoto City, 32.765147N, 130.687960E)

Fig. 10. A three-story building settled approximately by 50 cm (Karikusa, Minami-ku, Kumamoto City, 32.759882, 130.683249)

Fig. 11. Tilted buildings (Karikusa, Kamamoto City, 32.760014N, 130.682909E).

Fig. 12. Sand and gravel boil deposits. Maximum diameter of the gravel was 15 cm (Jin, Mifune-machi, 32.719221N, 130.770320E)

Fig. 13. Sand crater with a 110cm-diameter and 60cm-depth (Sasahara-machi, Uto City, 32.720672N, 130.611326E)

Fig. 14. Collapsed levee of the Kurokawa river and sand boils at the foot of the levee (Akamizu, Aso City, 32.926322N, 130.991291E)

Fig. 15. Sand boils in farmland (Okura, Aso City, 32.980056N, 131.083809E)

Fig. 16. Two-meters of settlement and lateral displacement of a farm road. Length of the settlement was approximately 50 m (Yakuinbaru, Aso City, 32.949986N, 131.084916E).

approximately 2,900 houses were damaged owing to liquefaction as of December 13, 2016 (Kumamoto-Nichinichi Shinbun, 2016); however, no details have been released for the other cities and towns. **Figures 5** through **16** show typical liquefaction-induced damage that occurred during the Kumamoto Earthquake.

4. Geomorphologic land classification of liquefied sites

Figures 17 and **18** show engineering-based geomorphologic land classification maps (7.5-arc-second JEGM) for the Kumamoto Plain and Aso region with superimposed liquefied sites, respectively. This type of map is used nationally for various kinds of hazard mapping in Japan (Wakamatsu and Matsuoka, 2013). Here, the land mass was classified into 24 geomorphologic units, as shown in the legend. Two major rivers flow across the Kumamoto Plain: Shirakawa River, which originates in Mt. Aso, and Midorikawa River, which originates in Mt. Sanpou-zan in the southeastern region of Kumamoto Prefecture.

The occurrence of liquefaction seems to be closely related to the geomorphologic units; for example, in the
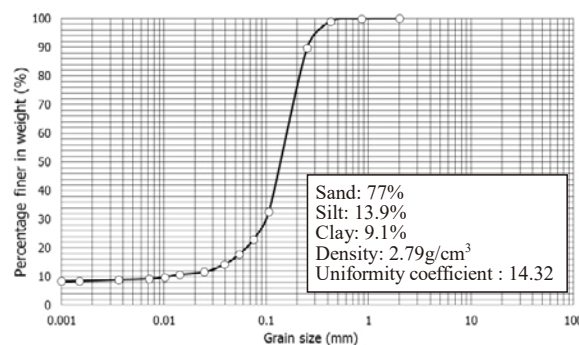
Fig. 19. Cumulative grain size distribution curve for sand boil deposit taken in Chikami, Minami-ku, Kumamoto City

Kumamoto Plain, the liquefaction is distributed in the flood plain, including the natural levee, back marsh, and former river channel, and in reclaimed land along the coast, whereas the liquefaction in the Aso region is distributed in the flood plain of Kurokawa River and in an alluvial fan located at the skirt of Mt. Aso.

Most of the sand boil deposits in the Shirakawa drainage basin appear to be secondary sediments of pyroclastic materials from Mt. Aso, known as "Yona," which are carried down by the rivers (**Figs. 5, 9 14,** and **15**). The typical grain size distribution of the sand boil deposit of Yona is shown in **Fig. 19**. To determine the grain size distribution, a soil sample was taken from sand boils in a well approximately ten days after the main shock by the owner of the well, as shown in **Fig. 7**, in Chikami, Minami-ku, Kumamoto City. The soil is classified as fine sand having a soil particle density of 2.79 g/cm^3 and a uniformity coefficient of 14.32, with a composition of 77.0% sand, 13.9% silt, and 9.1% clay.

In contrast, sand boil deposits with fine and large gravel were found in the Midorikawa drainage basin, and in Jin, Mifune-machi, gravel with a maximum diameter of 15 cm was ejected from farmland, as shown in **Fig. 12**. In the reclaimed land along the Ariake inland sea, sand boil deposits with shell fragments were observed, as shown in **Fig. 13**, which indicates that the marine sand deposits liquefied.

5. Effects of intensity of ground motion

Figures 20(a) and **(b)** show the distributions of the estimated peak ground acceleration (PGA) with a 250-m spatial resolution for the foreshock on April 14 and the main shock on April 16, respectively, superimposed with the liquefied sites during both shocks. The PGA for each 250-m grid cell was estimated based on a spatial interpolation procedure using the strong ground observation records (Matsuoka et al., 2015). The amplification factor of the PGA (Midorikawa et al., 2008) was calculated using the average S-wave velocity (Vs30)

196

K. Wakamatsu et al. / Lowland Technology International 2017; 19 (3): 191-202
Special Issue on: Kumamoto Earthquake & Disaster
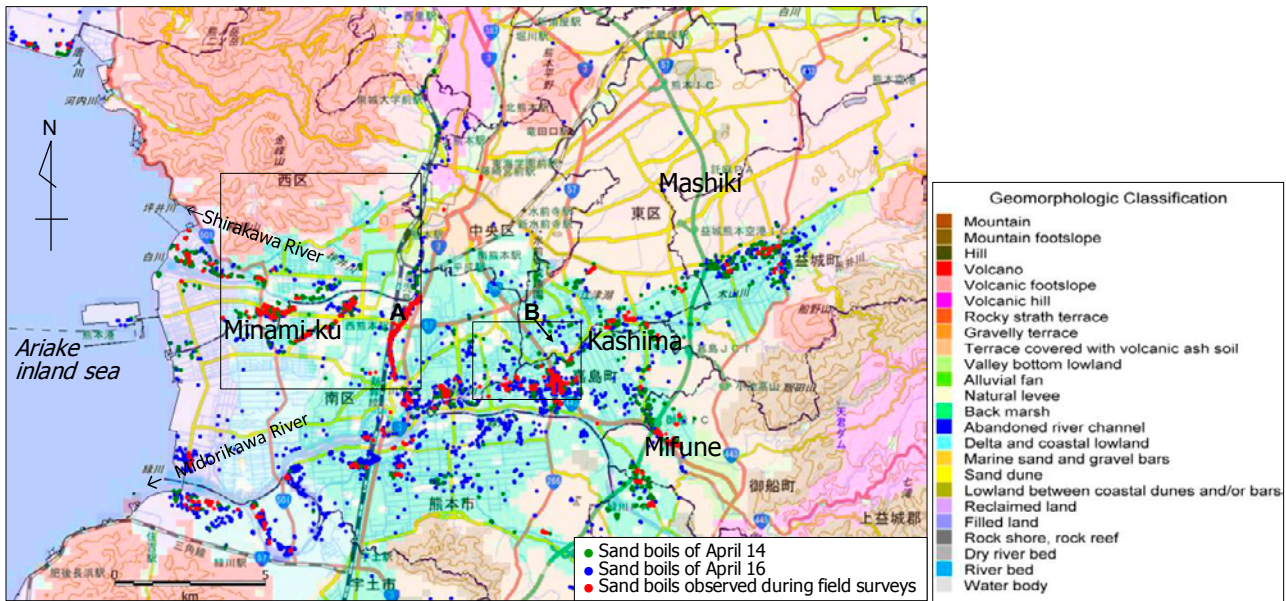
Fig. 17. Geomorphologic land classification map in Kumamoto Plain superimposing liquefied sites
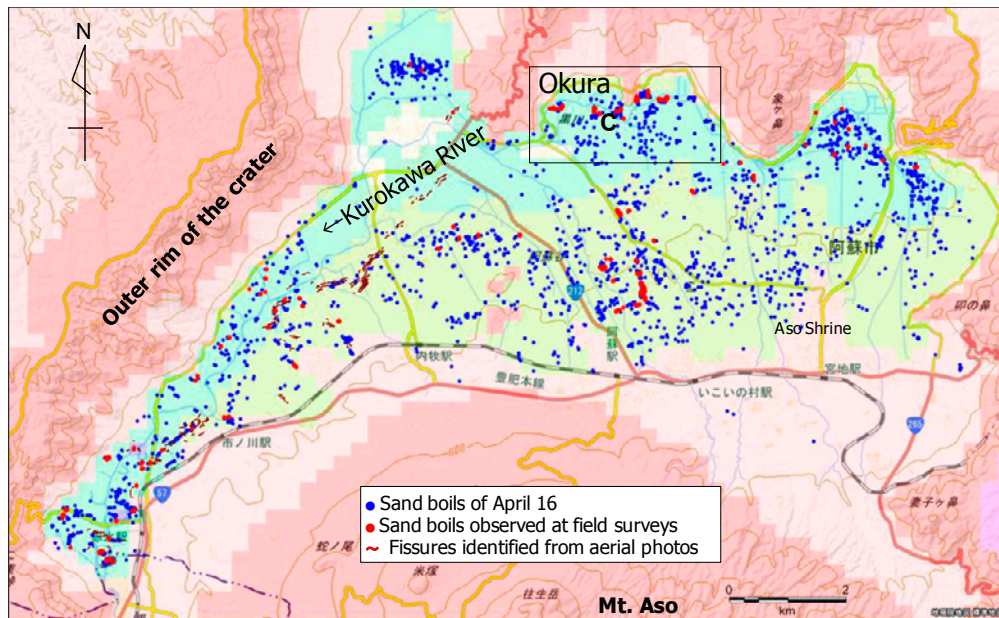
Fig. 18. Geomorphologic land classification map in Aso City superimposing liquefied sites (Explanation for geomorphologic land classification is the same as **Fig. 17**)

of the ground (Matsuoka et al., 2006) obtained from the 7.5-arc-second JEGM, which was used to estimate the acceleration on soft rock (Vs30, equal to 600 m/s). The spatial interpolation was then applied to determine the acceleration distribution on soft rock using a simple kriging, assuming a prior trend component, because the underlying random function model is the sum of the trend and residual components (Kawasaki Laboratory, 2008). The trend component (deterministic function) is assigned for the attenuation relation obtained on soft rock. Furthermore, the distribution of the PGA on the ground surface was calculated by multiplying with an amplification factor in the 250-m grid cell units.

Figures 21(a) and **21(b)** show the distributions of the estimated peak ground velocity (PGV) calculated in the same manner as the PGA for the foreshock and main shock, respectively, superimposed with the liquefied sites during both shocks.

The relationship between the number of liquefied grid-cells, and the PGA and PGV, was investigated with respect to the geomorphologic land classification, as shown in **Figs. 22(a)** and **22(b)**, respectively. It can be seen from the figures that liquefaction during the foreshock was induced when the estimated PGA and PGV exceeded approximately 100 cm/s^2 and 20 cm/s, respectively; however, during the main shock, liquefaction was induced by a lower PGV of 10 cm/s. The number of liquefied grid-

197

K. Wakamatsu et al. / Lowland Technology International 2017; 19 (3): 191-202
Special Issue on: Kumamoto Earthquake & Disaster

(a) Foreshock of April 14, 2016   (b) Main shock of April 16, 2016
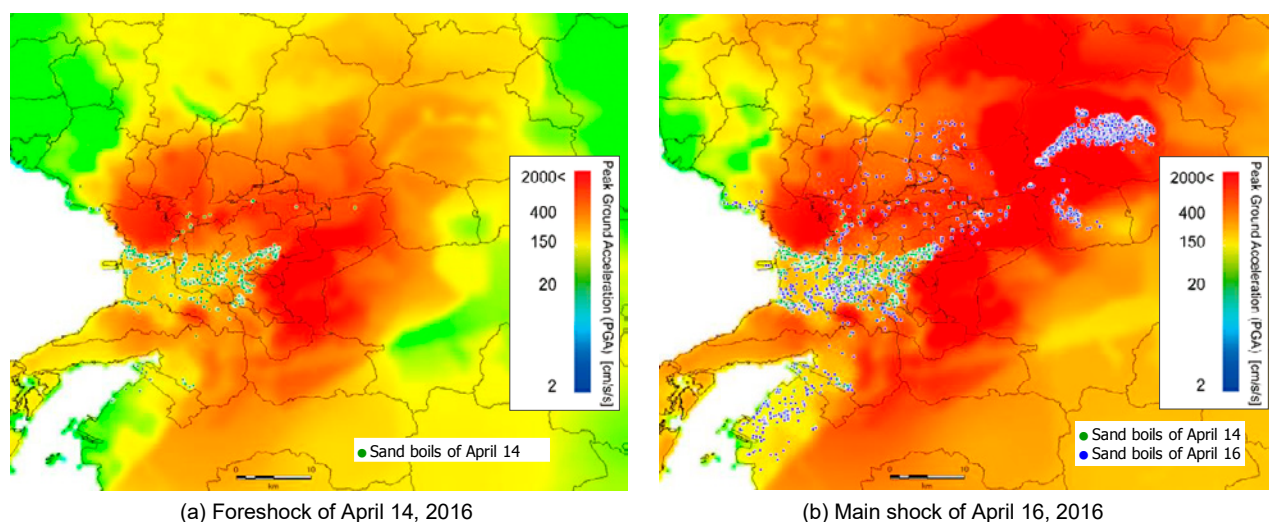
Fig. 20. Distribution of estimated peak horizontal ground acceleration and liquefied sites

(a) Foreshock of April 14, 2016   (b) Main shock of April 16, 2016
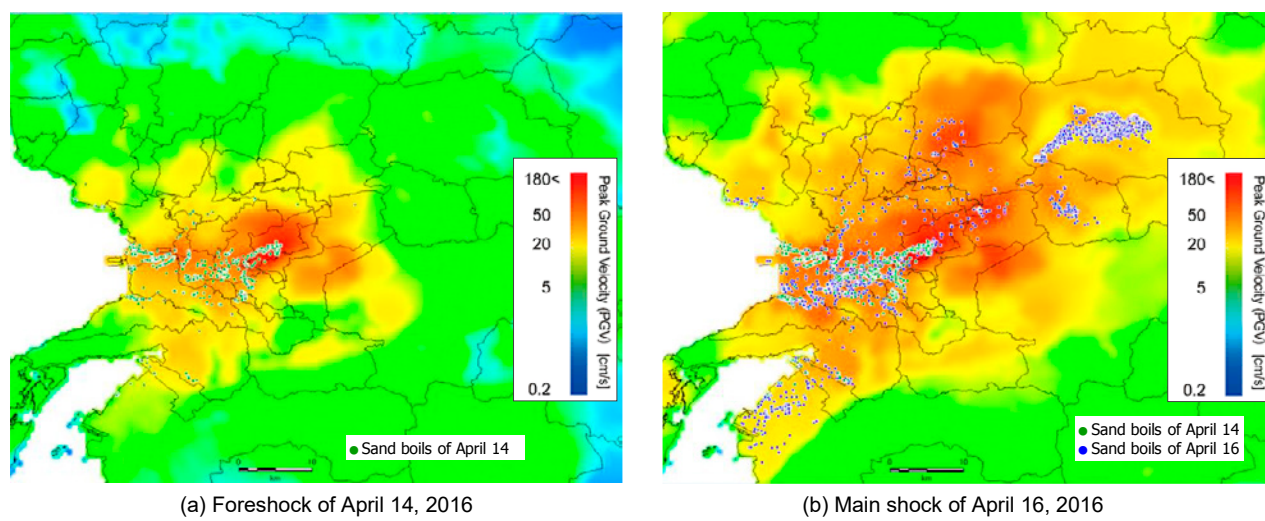
Fig. 21. Distribution of estimated peak horizontal ground velocity and liquefied sites

cells in back marsh is large, which is apparently due to the back marsh occupying a greater part of the Kumamoto Plain and Aso region. In contrast, the number of grid-cells in filled land, which is considered to easily liquefy, is remarkably low because the area of filled land is limited around Kumamoto Port.

Figures 23(a) and **23(b)** show the relationship between the liquefaction occurrence rate (number of liquefied grid-cells divided by the total number of grid cells) and the PGA and PGV levels, respectively, for geomorphologic units composed of Holocene deposits for the foreshock and main shock. It can be seen from **Fig. 23(a)** that the liquefaction occurrence rates for the main shock are remarkably higher than those for the foreshock for all PGA levels. The cause of this is thought to be the ground approaching a liquefied state during the foreshock, and easily liquefying owing to the lower intensity of the ground motion.

The rate of liquefaction is very low when the PGA is under 100 cm/s^2, but is relatively high when the PGA

ranges between 200 cm/s^2 and 700 cm/s^2, and a decrease with an increase in the PGA exceeding 800 cm/s^2. However, the rate rises sharply again when the PGA exceeds 2000 cm/s^2. Comparing **Fig. 22(a)**, geomorphologic units where liquefaction occurred in a range of PGA of between 200 and 700 cm/s^2 correspond to back marsh, natural levee, and delta regions, which are composed of soft soil. In contrast, the geomorphologic units where a range of PGA of between 800 and 2000 cm/s^2 correspond to the units which are composed of stiff soil such as volcanic footslope and volcanic hill. The PGA exceeded 2,000 cm/s^2 correspond to units composed of relatively hard soil, such as an alluvial fan, respectively.

In contrast, liquefaction was induced when the PGV exceeded 20 cm/s, and the rate gradually increased with an increase in the PGV level regardless of the geomorphologic units, as shown in **Figs. 22 (b)** and **23(b)**. The trends in **Figs. 22** and **23** seem to imply that the PGV is a more appropriate index for evaluating the liquefaction potential for a wide area, although further investigations

(a) Peak ground acceleration (PGA)

(b) Peak ground velocity (PGV)
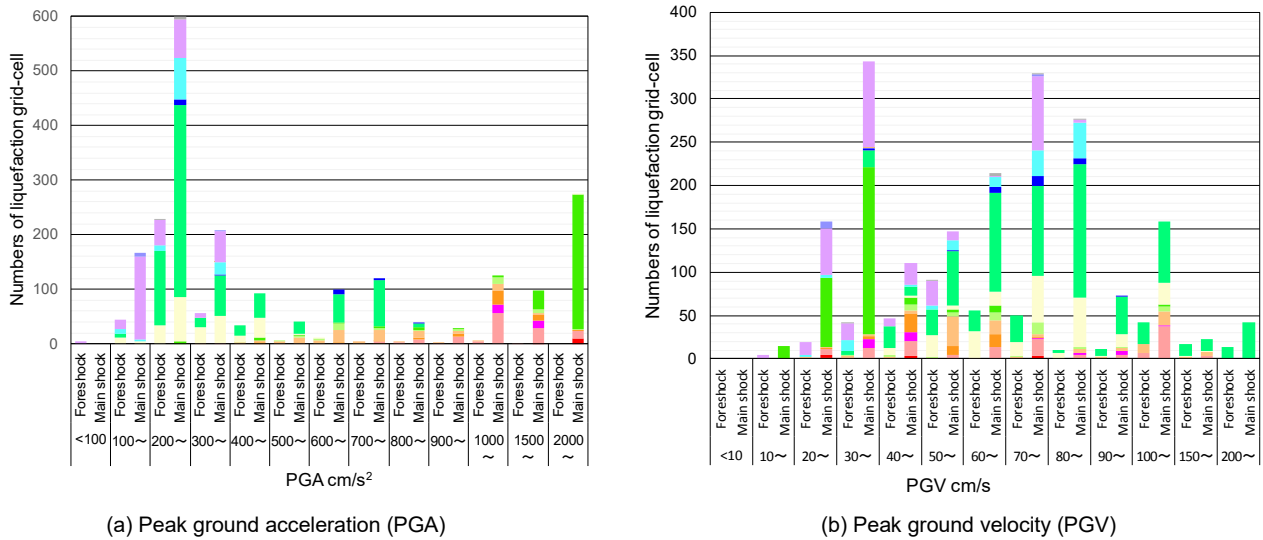
Fig. 22. Relationship between the number of liquefied grid-cells and levels of the intensity of ground motion for different geomorphologic units (Colors of the bar chart represent geomorphologic unit shown in the legend of Fig. 17)

(a) Peak ground acceleration (PGA)

(b) Peak ground velocity (PGV)
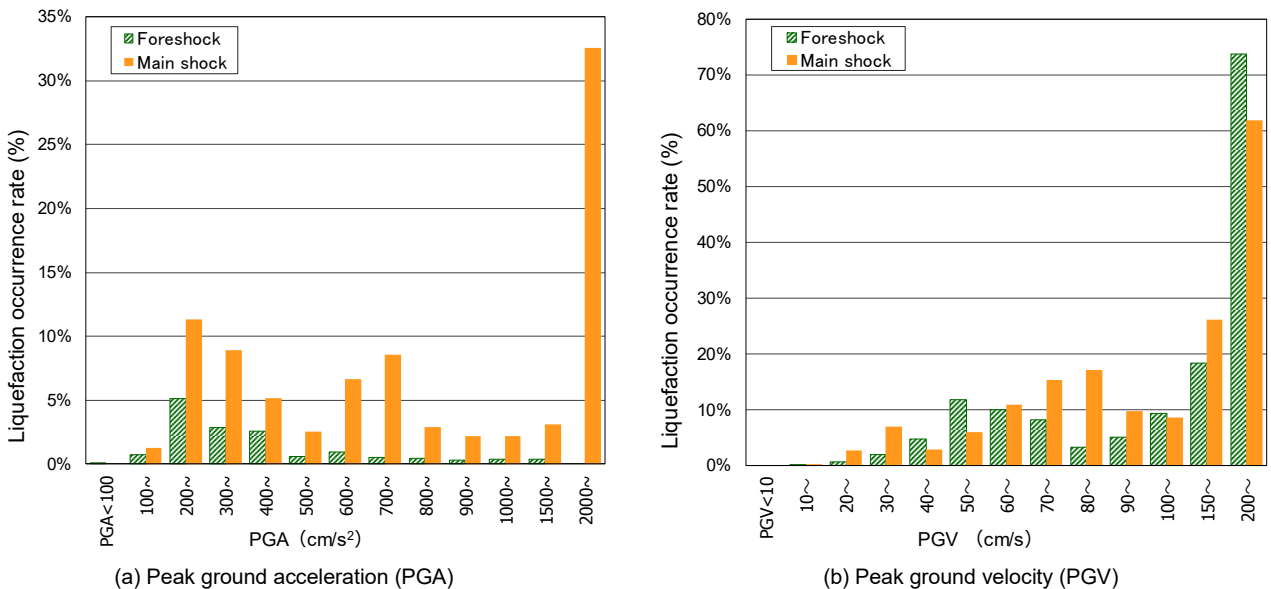
Fig. 23. Relationship between the liquefaction occurrence rate and levels of the intensity of ground motion for the main shock and foreshock

into many different case histories during earthquake events are needed.

6. Land conditions and soil profiles where widespread liquefaction occurred

The land conditions and soil profiles for three areas, Minami-ku, Kumamoto City; the town of Kashima-machi; and Okura, Aso City, where liquefaction (sand boiling) densely occurred, as shown in **Figs. 17 and 18,** are discussed below.

6.1 Minami-ku, Kumamoto City (Area A in Fig. 17)

Minami-ku, which is in the southern district of Kumamoto City, is located on the left bank of the Shirakawa River, as shown in **Fig. 17**. Long belt-like liquefied sites appeared along a small irrigation stream in Minami-ku (**Fig. 24**). Examples of the damage occurring in this area are shown in **Figs. 6** through **11**. The stream appeared to be a trace of a former large river channel; however, no land depression feature of the former river course was found. In addition, no large river was shown on older maps compiled around the years of 1605, 1650, 1700, 1838, or 1901.

199

K. Wakamatsu et al. / Lowland Technology International 2017; 19 (3): 191-202
Special Issue on: Kumamoto Earthquake & Disaster

Figure 25 shows the soil profiles and SPT N-value at point A, shown in **Fig. 24**, where significant sand boiling and differential settlement of the buildings occurred during both the foreshock on April 14 and the main shock on April 16, indicating loose fine sand consisting of "Yona" with very high-water content that is continuously present from near the ground surface to a depth of 8.5 m. The ground water level is at 1.0 m below the ground surface.

Using the simplified procedure to evaluate the factor of safety (F_L) against liquefaction, as presented in the Specification for Highway Bridges (Japan Road Association, 2002), sand layers from a depth of 1.0 to 17 m were found to be potentially liquefiable (i.e., with $F_L \leq 1.0$), as indicated by the blue and red colors in **Fig. 25**. For the evaluation, maximum horizontal accelerations of 355 cm/s^2 for the April 14 shock and 394 cm/s^2 for the April 16 shock at the ground surface (PGA), as indicated in **Fig. 20**, were adopted. The evaluation results for both shocks agree well with the actual performance of the ground, i.e., the thick liquefiable layer under the ground surface may have caused significant sand boiling and liquefaction-induced damage to homes during the foreshock and main shock.

6.2 Kashima-machi (Area B in Fig. 17)

The town of Kashima-machi lies in the center of the Kumamoto Plain, and sand boils were densely observed in the area between Kasegawa River and Midorikawa River, as shown in **Fig. 26**; however, the impact on the buildings was lower compared with in Minami-ku, as described in section 6.1. The area between the rivers is known to be a flood-prone zone, and in fact, acted as a flood-control reservoir until 2004 (Kumamoto River and National Highway Construction Office, 2016).

Liquefaction occurred mainly in a slightly elevated area by filling in low and wet back marsh in accordance with the land readjustment project between 1983 and 1998. It should be additionally noted that a shopping mall near Midorikawa River, shown in **Fig. 3**, was built on backfilled land after gravel mining to a depth of approximately 10 m in 1989.

Figure 27 shows the soil profile and SPT N-value at point B in **Fig. 26**. The sand beneath the ground surface was unexpectedly very thin at approximately 1 m. The soil from 3 m below the ground surface is a 6.7-m-thick gravelly soil with SPT N-values of approximately 20, which in turn overlie a 5.6-m-thick sandy soil layer with SPT N-values of around 10. The ground water level is at 2.4 m below the ground surface.

Using the simplified procedure to evaluate the F_L against liquefaction, sandy soil layers from a depth of 9 to 13 m were found to be potentially liquefiable for the April 16 shock, as indicated in red in **Fig. 27**; however, the liquefiable layers for the April 14 foreshock were thinner than for the April 16 main shock, as indicated in blue. For the evaluation, a PGA of 249 cm/s^2 for the April 14 foreshock and a PGA of 263 cm/s^2 for the April 16 main shock, as indicated in **Fig. 20**, were used. The evaluation results for both shocks agree with the actual ground performance, i.e., significant sand boiling occurred during the main shock on April 16, but had a minor impact on the foundation of a single-family home, and sparse sand boiling occurred during the foreshock on April 14.
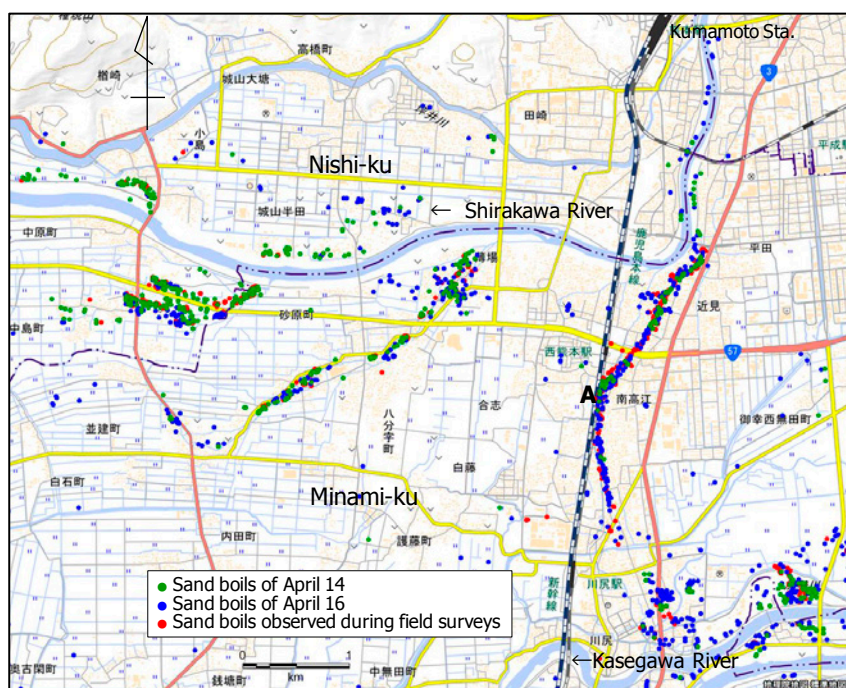
Fig. 24. Liquefied sites in Minami-ku, Kumamoto City
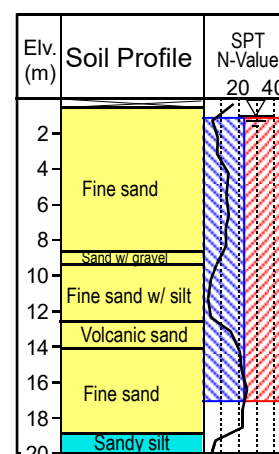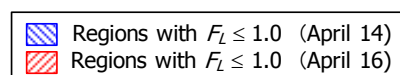
Fig. 25. Soil profile and SPT N-value in Hiyoshi, Minami-ku at Point A in Fig. 24
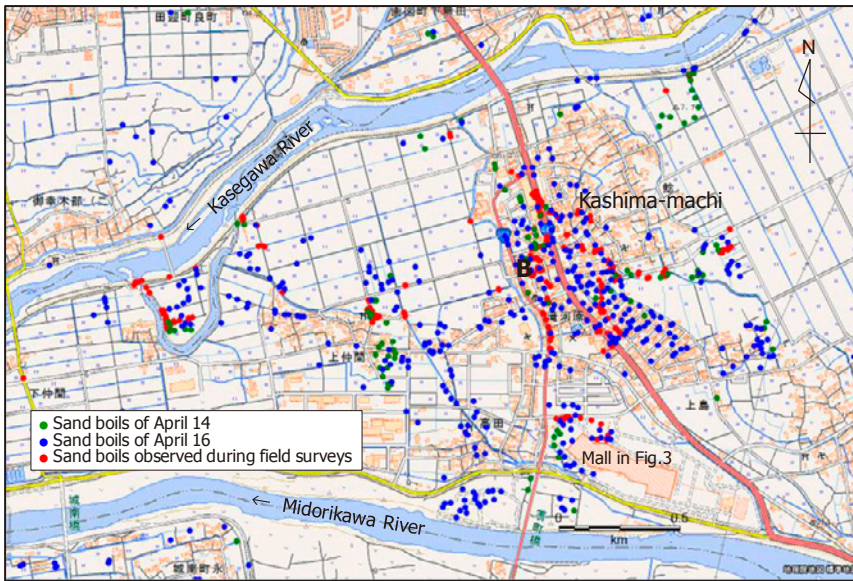
Fig. 26. Liquefied sites in Kashima-machi
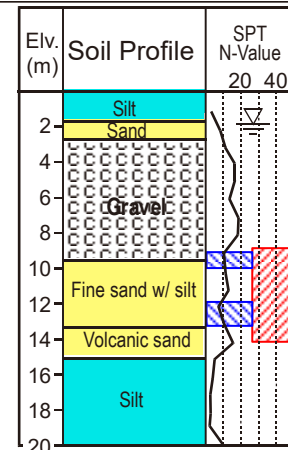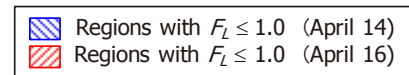
Fig. 27. Soil profile and SPT N-value in Kashima-machi at point B in Fig. 26
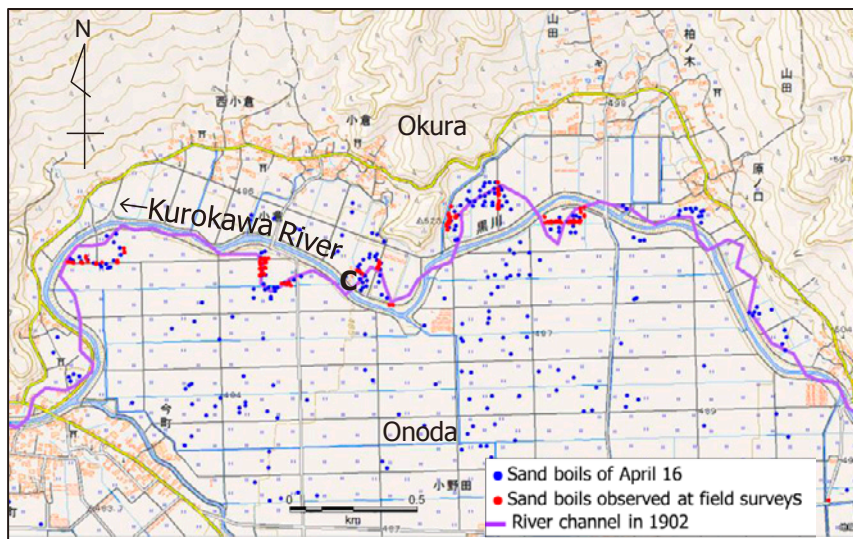
Fig. 28. Liquefied sites in Okura, Aso City
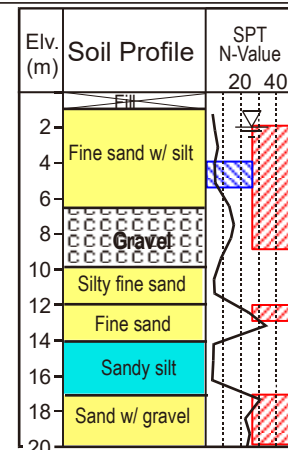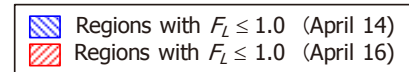
Fig. 29. Soil profile and SPT N-value in Okura, ASo Ciity at point C in Fig. 28

6.3 Okura, Aso City (Area C in Fig. 18)

Aso city is located approximately 40 km northeast of the Kumamoto Plain, and includes Mt. Aso, which is one of major active volcanoes in Japan. Liquefaction in the city was generated only from the main shock on April 16 within the caldera between Mt. Aso and the outer rim of the crater. In Okura, in the northern district of Aso, numerous sand boiling sites were observed along the former bent river channel, as shown in **Fig. 28**.

Figure 29 shows the soil profile and SPT N-value at point C, shown in in **Fig. 28**. A loose fine sand with silt assumed to be "Yona" lies from the ground surface to a depth of approximately 6 m. A 3.6-m-thick layer of sand and gravel with SPT N-values of around 10 lies beneath the sand. The ground water level is at 1.95 m below the ground surface.

Using the simplified procedure to evaluate the F_L against liquefaction, it was determined that sand and gravel layers are present from a depth of 2 to 9 m, and a 1-m- thick sand layer at a depth of 12 m was found to be potentially liquefiable from the April 16 shock, as indicated in red in **Fig. 25**; however, the liquefiable layers for the April 14 shock were only 2 m in height at a depth of 4 m, as indicated in blue. For the evaluation, a PGA of 183 for the April 14 shock and a PGA of 669 cm/s^2 for the April 16 shock, shown in **Fig. 20**, were used. The evaluation results for both shocks agree with the actual ground performance, i.e., significant sand boiling occurred during the April 16 shock, but negligible sand boiling occurred during the April 14 shock.

The land conditions, liquefaction, and analysis results

201

K. Wakamatsu et al. / Lowland Technology International 2017; 19 (3): 191-202
Special Issue on: Kumamoto Earthquake & Disaster

Table 1. Summary of land conditions, liquefaction, and result of analysis for areas where widespread liquefaction occurred

Place name	Land conditions	Liquefaction-induced damage		Thickness of liquefiable layers (Thickness of overlying unliquefiable layer)	
		Foreshock	Main shock	Foreshock	Main shock
Minami-ku, Kumamoto City	Natural levee	Significant	Significant	17m (1m)	17m (1m)
Kashima-machi	Fill in back marsh	Medium	Medium	3m (9m)	4m (9m)
Okura, Aso City	Former river channel	No	Significant	2m (4m)	11m (2m)

from the evaluation of the factor of safety (F_L) against liquefaction for three areas where widespread liquefaction occurred are summarized in **Table 1**. Both the thickness of the liquefiable layers with $F_L \leq 1.0$ and the overlying crust(i.e., liquefiable layer) seem to have affected the liquefaction-induced damage to the structures on the ground surface.

7.   Discussion and conclusions

Widespread liquefaction occurred within an 80-km-long zone, extending along the earthquake source faults in Kumamoto Prefecture, during a foreshock of the Kumamoto earthquake on April 14, 2016, and the main shock on April 16. Counting the numbers of grid cells containing liquefaction sites, as determined through the superimposing of 250-m grid cells, 404 and 1890 grid cells were designated as "liquefied grid-cells" for the foreshock on April 14 and main shock on April 16, respectively. Extensive damage was found in residential structures with a spread foundation, as well as in agricultural land and facilities, river levees, roads, and lifelines owing to the occurrence of liquefaction.

The most distant site from the epicenters of the foreshock and the main shock are Ohama, in Tamana City, and Ichinomiya, in Aso City, the epicentral distances of which are 29.6 and 42.6 km, respectively. Based on an empirical equation derived from past Japanese earthquakes, the distances during both the M_{JMA} 6.5 foreshock and M_{JMA} 7.3 main shock were not large with respect to the magnitude of the earthquake when compared with the distances from the epicenter to the farthest liquefied sites.

The occurrence of liquefaction appears to be closely related to the geomorphologic units. Liquefaction in the Kumamoto Plain was distributed in the flood plain including a natural levee, back marsh, and former river channel, and in reclaimed land along the coast, whereas liquefaction in the Aso region was distributed in the flood plain of Kurokawa River, and in an alluvial fan located at the skirt of Mt. Aso.

Most of the sand boil deposits in the Shirakawa drainage basin appeared to be secondary sediments of pyroclastic materials from Mt. Aso, known as "Yona." On the contrary, sand boil deposits with fine and large gravel

were found in the Midorikawa drainage basin. In the reclaimed land along the Ariake inland sea, sand boil with shell fragments of marine sand was observed.

Comparing the distribution of liquefied sites with that of the estimated PGA and PGV, liquefaction was distributed within those areas where the PGA exceeded approximately 100 cm/s^2 and the PGV exceeded approximately 20 cm/s. The rate of liquefaction (number of liquefied grid-cells divided by the total number of grid cells) for the main shock was remarkably higher than those for the foreshock for all PGA levels. The reason behind this is thought to be from the ground approaching a liquefied state during the foreshock, and easily liquefying owing to the lower intensity of the ground motion.

The rate of liquefaction is relatively high in the PGA ranging from between 200 and 700 cm/s^2, and then a decrease with an increase in the PGA exceeding 800 cm/s^2. However, the rate increased sharply again when the PGA exceeded 2,000 cm/s^2. This variation in the liquefaction occurrence rate versus the PGA appears to be due to the variation in geomorphological units. However, the rate gradually increases with an increase in the PGV level regardless of the geomorphologic units.

Based on an evaluation of the factor of safety (F_L) against the liquefaction, both the thickness of the liquefiable layers with $F_L \leq 1.0$ and the overlying crust (i.e., liquefiable layer) were shown to affect the liquefaction-induced damage to the structures on the ground surface.

References

Ambraseys, N., 1988. Engineering Seismology, Earthquake Engineering and Structural Dynamics, **17**: 1-105.

Geospatial Information Authority of Japan, 2016. High Resolution aerial photographs taken April 16 and April 20, 2016 in Kumamoto Prefecture.

Japan Road Association. 2002, Design specification of highway bridges –Part 5: Seismic design-, Tokyo, Japan, 121-125.

Kawasaki Laboratory, National Research Institute for Earth Science and Disaster Resilience, 2008. Free and Open Source Software, RASMO, Special project for earthquake disaster mitigation in urban areas, 2008.

Kuribayashi, E. and Tatsuoka, F. 1975., Brief Review of Soil Liquefaction during Earthquakes in Japan, Soils and Foundations, Japanese Geotechnical Society, **15**(4): 81-92.

Matsuoka, M., Wakamatsu, K., Fujimoto, K., and Midorikawa, S., 2006. Average shear-wave velocity mapping using Japan engineering geomorphologic classification map, Journal of Structural Engineering and Earthquake Engineering, Japan Society of Civil Engineers, **23** (1): 57s-68s.

Matsuoka M, Wakamatsu K, Hashimoto M, Senna S and Midorikawa S., 2015. Evaluation of liquefaction potential for large areas based on geomorphologic classification, Earthquake Spectra, **31**(4): 2375-2395.

Midorikawa, S., Komazawa, M., and Miura, H., 2008. Relationships between average shear-wave velocity and site amplification factors obtained by records from Yokohama dense strong-motion network, Journal of Japan Association for Earthquake Engineering, **8** (3), 19-30 (in Japanese with English abstract).

National Research Institute for Earth Science and Disaster Resilience, Hypocenter distribution map of the 2016 Kumamoto Earthquake, http://map03.ecom-plat.jp/map/map/?cid=20&gid=587&mid=2915, 2016.

Wakamatsu, K. 1991. Maps for Historic Liquefaction Sites in Japan, Tokai University Press, Hatano, Japan, pp 341 (in Japanese with English abstract).

Wakamatsu K, Kubo S, Matsuoka M, Hasegawa K and Sugiura M., 2005. Japan Engineering Geomorphologic Classification Map with CD-ROM Database, University of Tokyo Press, Tokyo, Japan: pp 104 (in Japanese with English abstract and manual).

Wakamatsu, K., 2011. Maps for Historic Liquefaction Sites in Japan with DVD-ROM Database, University of Tokyo Press, Tokyo, Japan: pp 90 (in Japanese with English abstract and manual).

Wakamatsu K. and Matsuoka M., 2013. Nationwide 7.5-Arc-Second Japan Engineering Geomorphologic Classification Map and Vs30 Zoning, Journal of Disaster Research, **8** (5): 904-911, Datum are available on line: http://www.j-shis.bosai.go.jp/JSHIS2/download.html? lang=en.

Cabinet Office, Japan (2016). Damage due to the Earthquakes Centered in Kumamoto Region as at 19:00 JST on March 14, 2017, http://www.bousai.go.jp/updates/h280414jishin/pdf/h280414jishin_38.pdf, (in Japanese).

The Headquarters for Earthquake Research Promotion, Japan (2016). Evaluation of the 2016 Kumamoto Earthquake, http://www.jishin.go.jp/main/index-e.html (in Japanese).

Kumamoto-Nichinichi Shinbun Co., Ltd., (2016), December 14, 2016 of Kumamoto-Nichinichi Shinbun, https://this.kiji.is/181571196170421753201 (in Japanese).

Kumamoto River and National Highway Construction Office, Kyusyu Reginal Development Bureau, Ministry of Land Infrastructure and Transport, Hapan, Kase-gawa River Improvement Project, http://www.qsr.mlit.go.jp/kumamoto/river/kaisyu/22kasegawa/7sagann/frame7.htm, (in Japanese).